Civil Engineering Infrastructures Journal 2022, 55(2): 259-276
DOI: 10.22059/CEIJ.2022.319629.1744

RESEARCH PAPER

Outrigger Braced System Placement Effect on Seismic Collapse Probability of Tall Buildings

Tavakoli, H.R.[1*], Moradi, M.[2], Goodarzi, M.J.[3] and Najafi, H.[4]

[1] Associate Professor, Department of Civil Engineering, Babol Noshirvani University of Technology, Babol, Iran.
[2] Ph.D. Candidate, Department of Civil Engineering, Babol Noshirvani University of Technology, Babol, Iran.
[3] Instructor, Department of Civil Engineering, Technical and Vocational University (TVU), Tehran, Iran.
[4] M.Sc. Student, University of Azad, Ghaemshahr Branch, Ghaemshahr, Iran.

Received: 23 Feb. 2021; Revised: 03 Jan. 2022; Accepted: 15 Jan. 2022

ABSTRACT: The placement of bracing can affect the seismic response and energy balance in the outrigger braced systems. In this study, it is attempted to investigate the effect of placement optimization of outrigger braced system on the seismic response of a 50-story structure. IDA curves are used to investigate the seismic responses. Sa and Sd are considered as intensity measure (IM) Parameters. Maximum story drift and inelastic strain energy considered as Engineering Demand Parameters (EDP). At first, IDA curves are derived based on maximum story drift in the structures. When the performance level is determined, their fragility curves are derived and compared. In the next step, the energy balance is investigated in the structures and the strain energy parameter is selected as EDP, which the damage level is determined in accordance with. Fragility curves are plotted and the results are assessed using the plastic strain energy. The results show that the placement optimization of outrigger braced system improves all structural parameters and reduces the collapse probability. Moreover, the fragility curves obtained from plastic strain energy as EDP are quite similar to the fragility curve derived from the selection of story drift as EDB.

Keywords: Fragility Curve, IDA Curve, Inelastic Energy, Outrigger Braced System, Tall Building.

1. Introduction

Outrigger braced structures have a central core consisted of shear walls or braced frames; the central core is attached to the outer columns by outrigger trusses or girders (Ding et al., 2018). When the structure is subjected to lateral loads, rotations of the core are restrained by the outriggers through tension in windward columns and compression in leeward columns (Gorji and Cheng, 2017). Given the considerable effective depth of these structures, the lateral stiffness increases and the lateral displacement and moment of the core decline significantly (Gorji and Cheng,

* Corresponding author E-mail: tavakoli@nit.ac.ir

2017). Outrigger braced structures are used for buildings of 40 to 70 stories. If the lateral resistance system of a structure is merely based on a braced core, its deformation under a lateral force is like that of a cantilevered beam in the bending mode; but if the core is connected to the outer columns by a relatively stiff truss (outrigger braced system), the rotation of the core under lateral loading causes the rotation of outrigger braced system and the outer columns are tensioned on one side and compressed on the other side. This process involves columns in lateral load-bearing. In this case, the core approximately shows an S-shaped deformation (Zhao et al., 2017).

Involving the columns, the performance of outrigger braced system reduces the moment of the core and axial forces of core columns under lateral loading, although it does not affect the core shear and shear loads must be entirely borne by the core. The performance of outrigger bracing in structural core is like the performance of torsion spring on a cantilevered beam under distributed loading (Patil and Sangle, 2016). The concentrated moment applied by the spring reduces the moment of cantilevered beam and displacement of its tip.

Using compatibility equations of a cantilevered beam and a torsion spring based on linear elastic behavior and uniform cross-section, Stafford Smith and Coull (1991) found that the tip displacement function of the beam can be expressed in terms of the distance between the tip of the beam and the location of torsion spring and the optimal location of spring can be determined by its derivative with respect to x in order to minimize the tip displacement of the beam. Various research has been done in this regard. Tan et al. (2015) studied Dynamic characteristics of energy dissipation systems with damped outriggers. Lee and Tovar (2014) studied outrigger placement in tall buildings using topology optimization. (Jiang et al., 2017) studied seismic performance of high-rise buildings with energy-dissipation outriggers. Mashhadiali and Kheyroddin (2014) studied progressive collapse assessment of new hexagrid structural system for tall buildings. They illustrate that resisting progressive collapse capacity, in both hexagrid and diagrid structures, is increased by using the buckling-restrained elements. He and Lu (2019) studied seismic fragility assessment of a super tall building with hybrid control strategy using IDA method.

Studies on the fragility analysis using Peak Ground Velocity (PGV) demonstrate that, for tall buildings, PGV is not only suitable for IDA but also works well in fragility analysis based on its high efficiency and reasonable exceeding probabilities. Mashhadiali and Kheyroddin (2013) studied on proposing the hexagrid system as a new structural system for tall buildings. According to the results, the hexagrid system has a better architectural view and more ductility and stiffness sensitivity, which are about three times than that of the diagrid system. Finally, in comparison with the diagrid system, the hexagrid system has enough potential to push the height limit.

In this study, a 50-story structure is designed with an outrigger braced steel core system. Structures are considered in both modes of the original structure and the structure optimized in terms of outrigger braced system placement. The study is mainly aimed to evaluate the response of structures during near-field earthquakes.

1.1. Performance-Based Earthquake Engineering (PBEE) Provisions

Fragility curve commonly described by using a log-normal CDF, whose characteristic parameters are C and β collected in the vector ϑ = (C,). In particular parameter C: is the intensity measure producing 50% of failure (median) and β: is the logarithmic standard deviation describing the dispersion of results due to both record-to-record variability and uncertainties about the system response. Therefore, the conditional probability of failure can be obtained by the convolution

integral $P_f(v) = \int_R F_C(i,v) f_I(i) di$; where R+ represents the set of positive real numbers and *i*: is the intensity (Dall'Asta et al., 2021).

The fragility curve is plotted for the structure by drawing different values of Probability for each IM (Mobinipour and Pourzeynali, 2020). These curves indicate the increasing probability of damage conditions for structures exposed to earthquake. Engineering demand parameters are generally considered as story drift, axial deformations of column and plastic hinges rotations. Various parameters such as PGA, PGD, PGV, spectral acceleration (Sa), etc. are also considered for intensity measure (Nazari and Saatcioglu, 2017). To assess the PBEE, a set of analyses must be conducted using Incremental Dynamic Analysis (IDA) (Asgarian and Ordoubadi, 2016). IDA involves a set of nonlinear dynamic analyses under a series of scaled earthquake records whose intensities should ideally cover the entire range from elasticity to general dynamic instability. In this study, the maximum story drift and plastic strain energy dissipated in each structure are considered as EDP and the spectral acceleration (Sa) and spectral displacement (Sd) are considered as IM.

1.2. Plastic Strain Energy in the Structure

The seismic energy input applied to the structure can be converted into a set of internal energies. Strain energy, kinetic energy (E_k) and the energy dissipated by structural damping (E_ξ) are a set of internal energies in structure, mobilized against the input energy (E_i). The strain energy is divided into elastic strain energy (E_e) and plastic strain energy (E_{in}) in the structure. According to Eq. (1), input energies and internal energies are balanced in the structure:

$$E_i = E_k + E_\xi + E_e + E_{in} \quad (1)$$

$$E_k = \frac{m\dot{u}^2}{2} \quad (2)$$

$$E_\xi = \int C\, \dot{u}^2 dt \quad (3)$$

$$E_e + E_{in} = \int f_s du \quad (4)$$

$$E_i = -\int m\ddot{u}_g du_g \quad (5)$$

where *m*: is mass of the structure, *C*: is the damping coefficient, f_s: is the restoring force, *u*: is the displacement of the mass, u̇: is the velocity of the mass, $\ddot{u}$: is the acceleration of the mass, u_g: denotes the foundation displacement, and *t*: is time (Jamnani et al., 2018).

If the sum of elastic strain energy, energy dissipated by damping and kinetic energy is not balanced with the input energy, the structure uses the plastic strain energy to reach an energy balance (Shin and Kim, 2016). Plastic strain energy causes permanent deformations and damages in the structure (Tavakoli and Afrapoli, 2018). Therefore, if energy is used as a criterion for assessing the seismic performance of structure, plastic strain energy can be considered as EDP which can lead to a damaged in the structure if exceeds the IM.

As stated previously, in this study, a 50-story structure is considered in both original mode and the optimized outrigger braced structure to evaluate their behavioral differences, performances and failures during near-field earthquakes. In this study, IDA (Mohammadizadeh and Jafarzadeh, 2021) and fragility curves are used to achieve the research objectives. The parameters Sa and Sd are considered as IM and the maximum story drift and plastic strain energy are considered as EDP to derive IDA and fragility curves. The specification of proposed models, the seismic loading and the research results are then presented.

2. Introduction to Original Structural Model

In this study, a 50-story structure is modeled and designed initially for time history dynamic analysis. For designing this

structure it was assumed that the structure has a 49 × 49 m plan in the 1st to 5th stories, 35 × 35 m plan in the 6th to 26th stories, 28 × 35 m plan in the 27th to 41st stories and 21 × 35 m plan in the 42nd to 50th stories. The height of stories is considered constant, equal to 3.7 m (Figure 1). The dead load is 700 Kgf/m^2 for the structure and the live load is also considered 350 Kgf/m^2 for the 5 first floors and 200 Kgf/m^2 for other floors. The snow load is 150 Kgf/m^2 for the proposed structure. The ASCE (2016) is employed for the loading. The base wind speed is considered 41.7 m/s for the region in Iran. The structure is designed for both seismic and wind loads. A spectral dynamic analysis is used for the seismic analysis. It is assumed that the structure is located in a high-risk seismic zone with a peak ground acceleration of 0.3 g, on the soil type 2. Since the Iranian Seismic Code No. 2800 is used for seismic loading and it does not provide behavioral and dynamic magnification factors for outrigger braced structures, linear and nonlinear modeling are applied simultaneously for structural design. Figure 1 Shows the flowchart of design procedure.

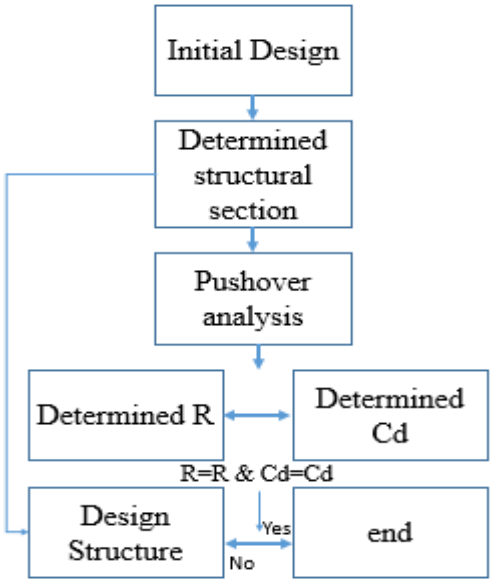

Fig. 1. Design flowchart

After initial design of the structure, the behavioral factor and displacement amplification factor (Cd) are calculated and the design is modified and this process continues until achieving convergence (4 steps). In Table 1, behavioral and Cd factors are shown for the design steps. The ST37 steel with yield stress of 2400 kg/cm^2, specific weight of 7850 Kg/m^3 and ultimate stress of 3700 Kg/cm^2 is used.

Table 1. Determining the values of R and Cd factors

Step	Cd	R	Outrigger braced placement
1	2.17	2.32	Original
2	2.5	2.45	Original
3	2.65	2.59	Original
4	2.69	2.61	Original
5	2.71	2.68	Optimized

2.1. Determining Optimal Placement of Outrigger Bracing

The structure is analyzed and designed after the loading and appropriate sections are then derived. In initial design of the structure, it is assumed that the outrigger braces are placed on the roof and the middle of the structure. Then, the structure is designed. In design process, box sections are used for column and bracing elements and I-shaped sections are used for beams. The suitable sections are shown in Table 2. Figure 2a shows the modeling of original structure. The original structure is designed and then exposed to the triangular load applied by wind and earthquake to calculate the optimal displacement of outrigger bracing. In calculations of the outrigger bracing assumed that the structure behaves linearly, just axial forces are borne by the columns and the outrigger brace connected to the core and columns using fixed and pinned connections, respectively. The geometric properties of the core, columns and outrigger truss are assumed fixed along the height and the lateral load is considered for triangular mode.

Accordingly, in this research assuming two outrigger braces, the ratio of optimum outrigger bracing placement to the entire height of structure (x/H) is calculated 0.52 and 0.188 using the equation. Therefore, the placement of braces is shifted to upper stories 42 and 41 as well as middle stories 26 and 25 in the optimized structure

Table 2. Structural sections in original model of 50-story structure

Story	Column (Box) (cm)		Brace (Box) (cm)		Beam	
	Core	Other	Outrigger	Core	Outrigger	Other
1-5	200×10	80×35		100×5		IPE 300
6-20	180×8	80×3		100×5		IPE 300
20-25	150×7	80×3		80×4		IPE 300
25-30	150×5	70×3	100×5	80×4	HEA 1000	IPE 300
30-35	120×4	50×3		80×4		IPE 300
35-40	80×3	40×2		80×3		IPE 300
40-45	80×3	35×2		60×3		IPE 300
45-50	80×3	30×1	80×2	60×2	HEA 1000	IPE 300

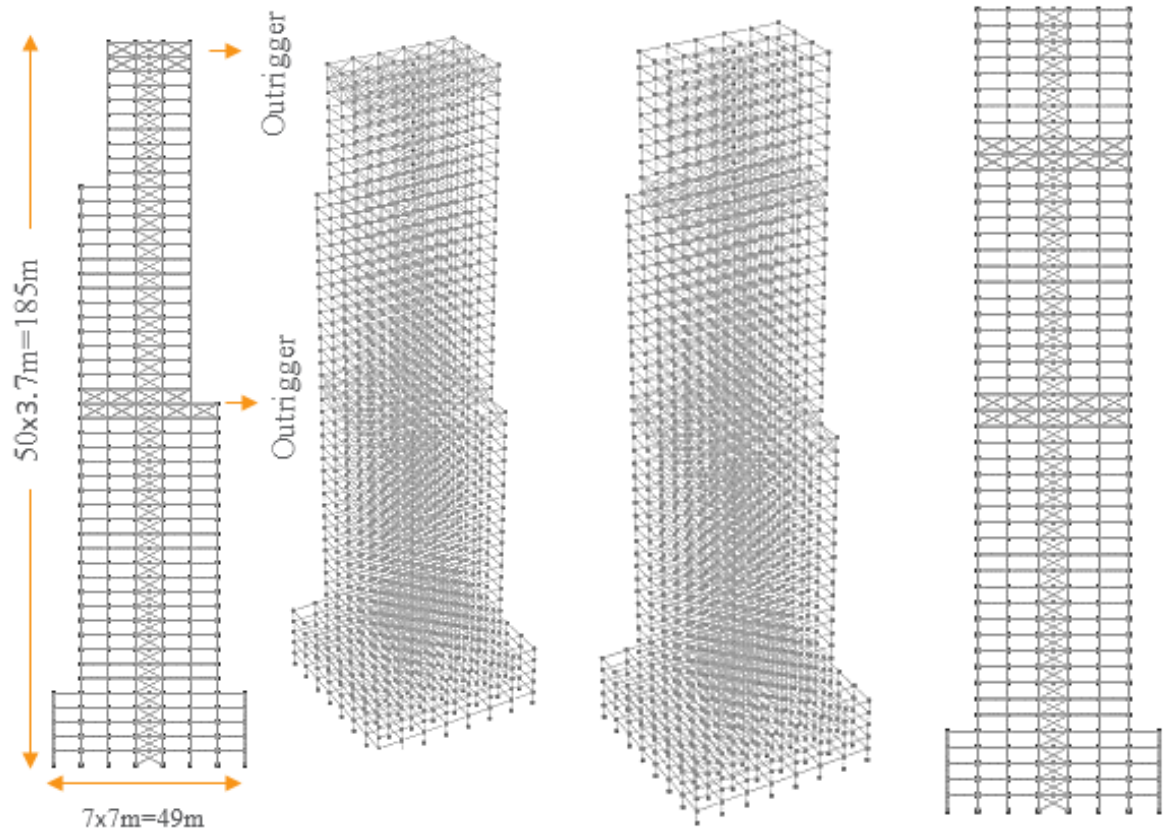

(a) **(b)**

Fig. 2. Finite element models of 50-story outrigger braced structure: a) Original model; and b) Optimized outrigger braced model

2.2. Nonlinear Modeling

The proposed structure is modeled by Perform-3D software for the nonlinear dynamic time history analysis. A concentrated plastic hinge is used for the nonlinear modeling. Force-displacement relationships are defined for beam, column and bracing elements based on the FEMA 356 (FEMA, 2000). FEMA-Beam element is used for nonlinear modeling of the beams and FEMA-Column element is employed to model the columns. A schematic of plastic hinges is shown in Figure 3, according to the FEMA 356. In Table 3, the modeling parameters and performance levels are shown for the elements. To evaluate the seismic performance of the structure using the plastic hinges rotation, three limit modes have been defined. The three performance levels including Immediate Occupancy (IO), Life Safety (LS) and Collapse Prevention (CP) have been selected as criteria for low, medium and high failure, respectively, based on different references (Jiang et al., 2017).

2.3. Seismic Loading

In this study, 18 earthquakes are used for seismic analysis. The characteristics of records are listed in Table 4. The records are

scaled up and applied to the structures. At first, the acceleration response spectrum and the displacement response spectrum are extracted. In Figure 4, the acceleration response spectrum (for a damping ratio equal to 5%) and its corresponding displacement response spectrum are shown in the periods of both structures. Since the structure has a long period, the acceleration response spectrum (Sa) of the structure shows that it has a low sensitivity to the acceleration values. However, a comparison of Sa and Sd values indicates that the structure has a very high sensitivity to the values of acceleration spectrum.

Different authorities introduce different seismic parameters for IM, each with its own characteristics. However, Sd indicates the displacement response of the system is one degree free and is used in tall structures that are more sensitive to displacement than acceleration. But in general, the acceleration response parameter is a fundamental parameter that gives an easier understanding of the magnitude of the earthquake. Therefore, both Sd and Sa have been used in this research.

To reach a reasonable response in this study, the structural responses are investigated as a function of Sa and Sd values in the incremental dynamic analysis. Because it seems that the acceleration response spectrum (Sa) does not change significantly as the PGA rises, but the displacement response spectrum values increase much more. Therefore, it is more reasonable to use the displacement response spectrum to explain and compare the results, but the responses of structures to the both parameters Sa and Sd are examined for a better comparison.

Table 3. Modeling values and performance levels for definition of plastic joints in structural members based on FEMA 356

Component type	Characteristic parameters			Deformation limit		
	a	b	c	IO	LS	CP
Column	$9\theta_y$	$11\theta_y$	0.6	$1\theta_y$	$6\theta_y$	$8\theta_y$
Beam	$4\theta_y$	$6\theta_y$	0.2	$0.25\theta_y$	$2\theta_y$	$3\theta_y$
Bracing in compression	$0.5\Delta_c$	$8\Delta_c$	0.2	$1.25\Delta_c$	$6\Delta_c$	$8\Delta_c$
Bracing in tension	$11\Delta_T$	$14\Delta_T$	0.8	$1.25\Delta_T$	$8\Delta_T$	$10\Delta_T$

Table 4. Specifications of earthquake records considered for incremental dynamic analysis (IDA) (Tajammolian et al., 2018)

No.	Record	Station	Max. PGA (g)	Mw
1	Cape Mendocino	Cape Mendocino	1.43	7
2	Chi-Chi, Taiwan	TCU084	1.16	7.6
3	Chi-Chi, Taiwan	TCU065	0.789	7.6
4	Coalinga-05	Oil City	0.841	5.8
5	Gazli, USSR	Karakyr	0.71	6.8
6	Imperial Valley-06	Elcentro#5	0.528	6.5
7	Imperial Valley-06	Elcentro#8	0.602	6.5
8	Kocaeli, Turkey	Izmit	0.22	7.5
9	Loma Prieta	BRAN	0.64	6.9
10	Morgan Hill	Coyote Lake Dam	1.3	6.2
11	Nahanni	Site 2	0.45	6.8
12	Northridge	Converter Station	0.897	6.7
13	Northridge	Sylmar	0.843	6.7
14	San Fernando	Pacoima Dam	1.24	6.6
15	Bam	Bam	0.8	6.6
16	Tabas	Tabas	0.85	7.35
17	Manjil	Abhar	0.51	7.37
18	Duzce	Bolu	0.822	7.1

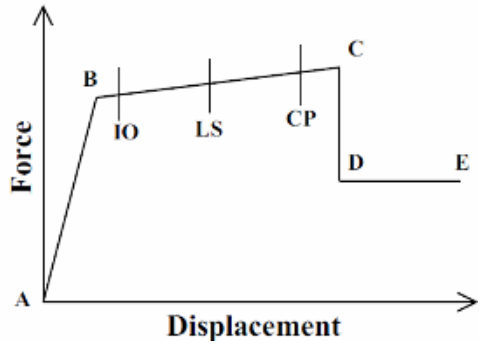

Fig. 3. Modeling parameters and performance levels in plastic joints based on FEMA 356 (Jiang et al., 2017)

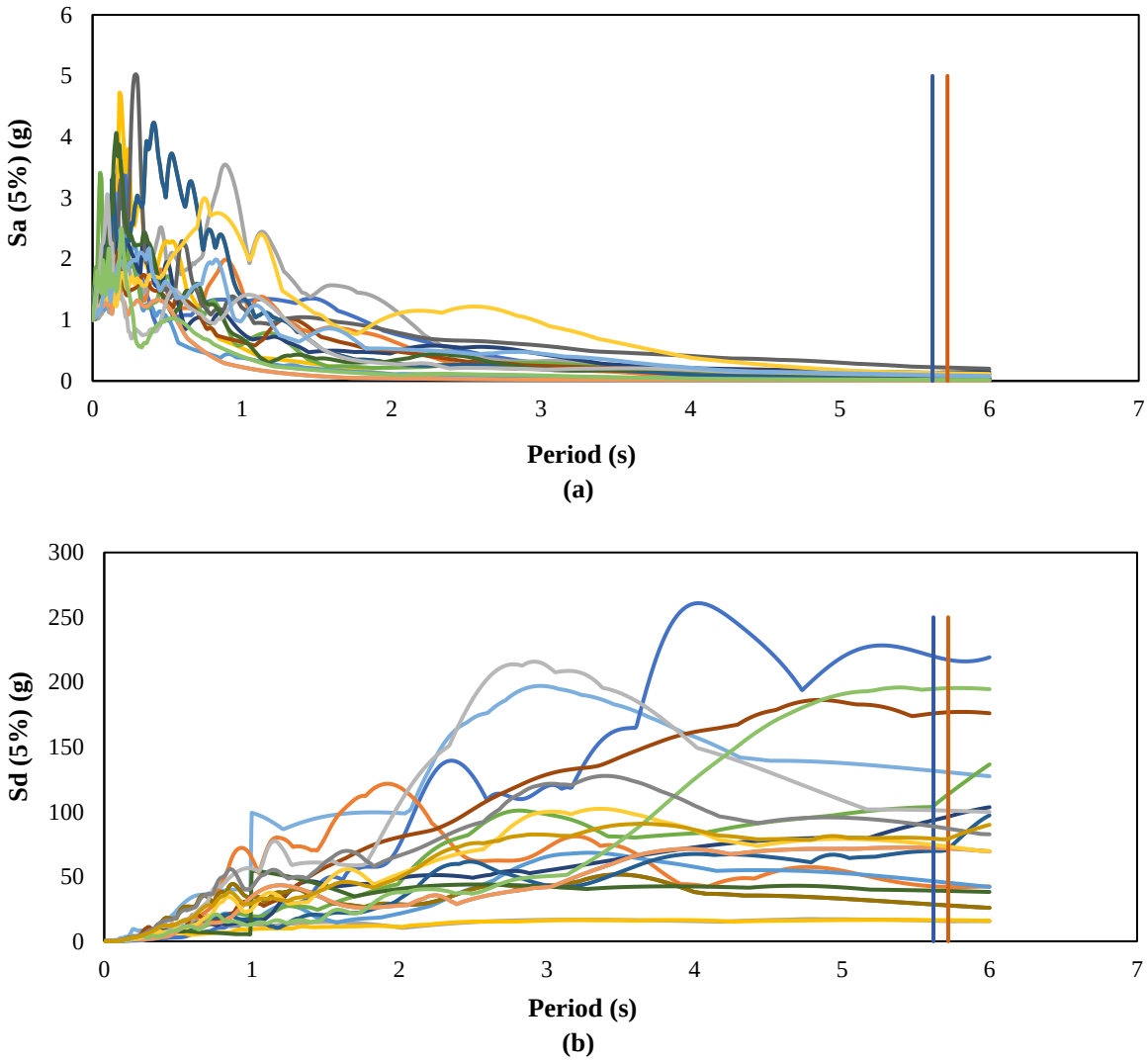

Fig. 4. Spectral response: a) Acceleration spectrum; and b) Displacement spectrum

3. Results of Analysis

After nonlinear modeling, outrigger braced structures are subjected to the dynamic seismic load in both original and optimized conditions in order to evaluate their responses. The dynamic load is applied to structures incrementally and the drift and plastic strain energy are derived as research parameters and presented based on parameters Sa and Sd. Initially, the performances of structures are partially compared in some particular earthquakes.

At first drift ratio curves for Chi-Chi earthquake with PGA of 0.2 to 1.4g are illustrated (in 0.2g steps in X and Y

directions for both structures) (Figures 5 and 6). Then rotations of plastic hinges are compared. The results of analysis show that the 47th stories experiences the maximum drift during the earthquake in both structures. As the PGA rises, the response of the structure and the drifts increase. This increase is more in the original structure than the optimized outrigger braced structure. The optimization of outrigger bracing placement causes maximum acceleration of the structure at the applied PGAs to be less than the original structure. Maximum drift is a symbol of structural stability, so the structure is more stable if the outrigger is placed in its optimum position. In addition, the results show that as outriggers are less spaced apart, the drifts between two outriggers are reduced. In fact, reducing the distance between two belts and inserting an outrigger belt in the middle of the structure decrease the total drift of the structure as well as the story drift between two belts. In Figure 7, the plastic hinge rotations are compared at LS performance level (red elements) during Chi-Chi earthquake at PGA = 1g. The results show number of hinges reach to the LS performance level in optimized structure is less than the original structure. In fact, the role of outrigger bracing in reducing the torsion of steel core causes the optimized outrigger braced structure to perform better than the original structure.

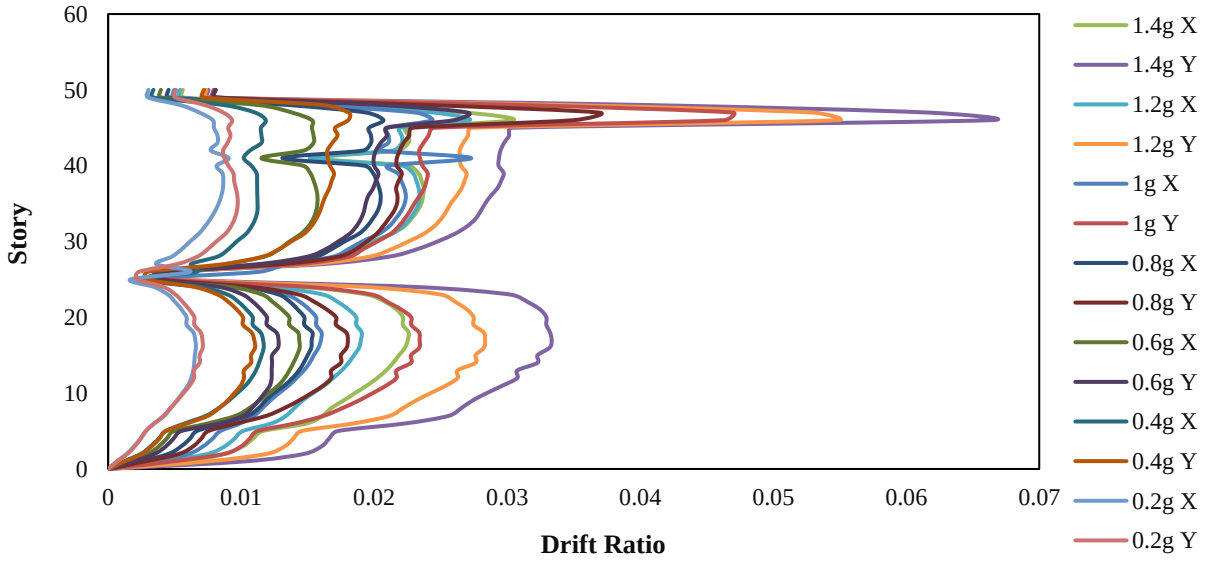

Fig. 5. Maximum story drift curve for original structure under Chi-Chi earthquake

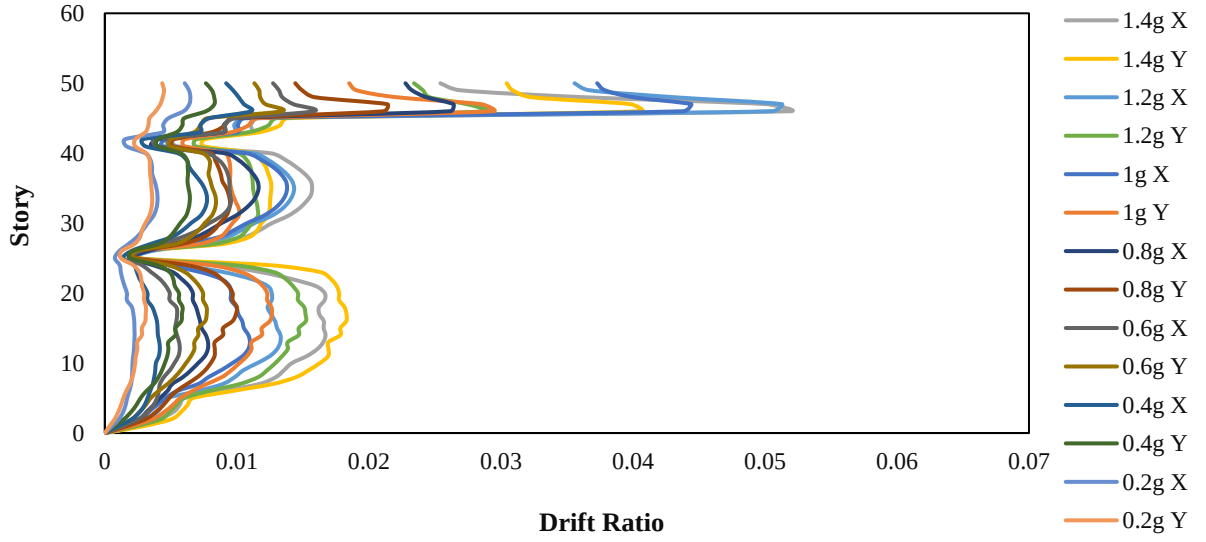

Fig. 6. Maximum story drift curve for optimized outrigger braced structure under Chi-Chi earthquake

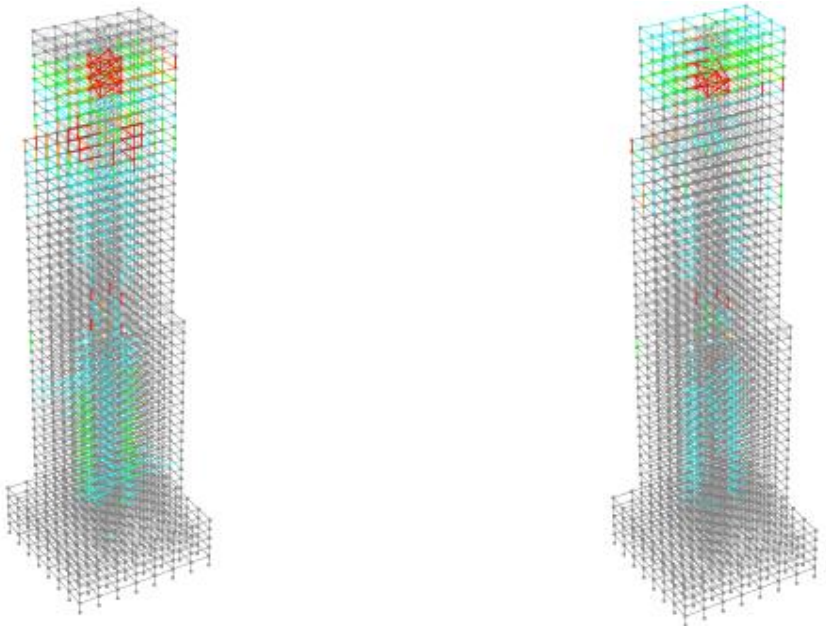

(a) **(b)**

Fig. 7. Rotation of plastics hinges at LS performance level in Chi-Chi earthquake with PGA = 1g: a) Original structure; and b) Optimized structure

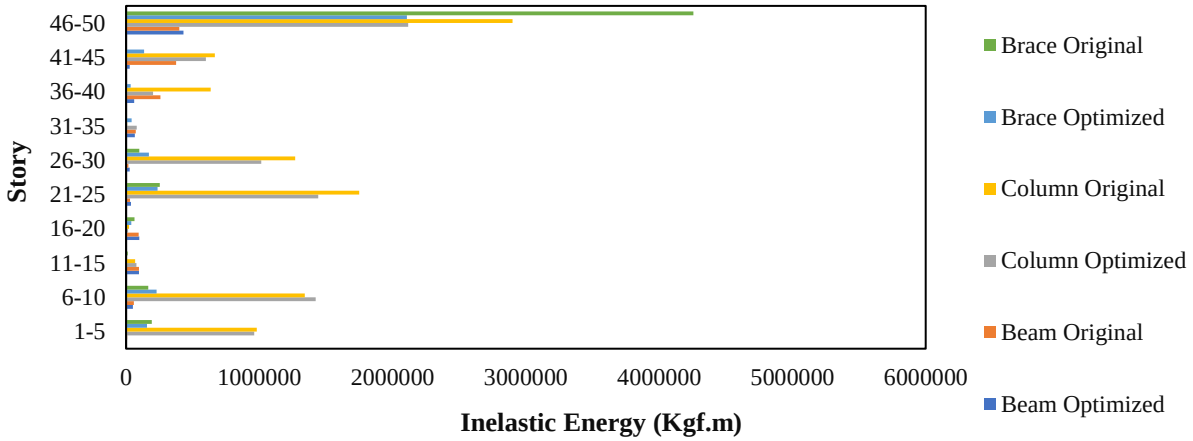

Fig. 8. Plastic strain energy in original and optimized structures in Chi-Chi earthquake with PGA = 1g

Figure 8 represents the dissipated strain energy for beam, column and bracing elements in the both structures. According to the figure, the highest dissipated strain energy is observed in the steel core braces and columns. The beams have the least plastic strain energy. In fact, the steel core in the center of structure causes the strain energy of other elements to be negligible and the structural damage to be minimized in other elements. An investigation into plastic strain energy in the original and optimized outrigger braced structure shows that the strain energy dissipated in the original structure is usually more than that of the optimized structure. In fact, transferring the braces to the optimal position reduces plastic strain energy and, consequently, decreases structural damage due to the earthquake. The IDA curves are presented for the proposed structures. Initially, the drift curves are presented for different values of Sa and Sd. Figure 9 demonstrates the IDA curves for the drift parameter in both original and optimized outrigger braced structures. According to the figure, as Sa and Sd increase, maximum drifts rise to reach the failure boundary; in the failure boundary, drift values significantly surge as the Sa and Sd increase slightly. An investigation of fragility curves shows that the structure experiences stiffening and softening irregularly as IM values increase. This means that the

structure sometimes is faced with a decrease in EDP as IM increases (Sa and Sd). This can be a positive factor for increasing the structural strength and preventing damage. In fact, in these structures, the structural performance is a non-uniform function of IM growth. When an ultimate softening zone emerges in the IDA curve, a dynamic instability is created in the structure. Generally, the mean or median is used to sum up IDA curves. In this study, the median IDA curves are employed to better evaluate and compare the IDA curves. In Figure 10, the median IDA curves are presented for both structures.

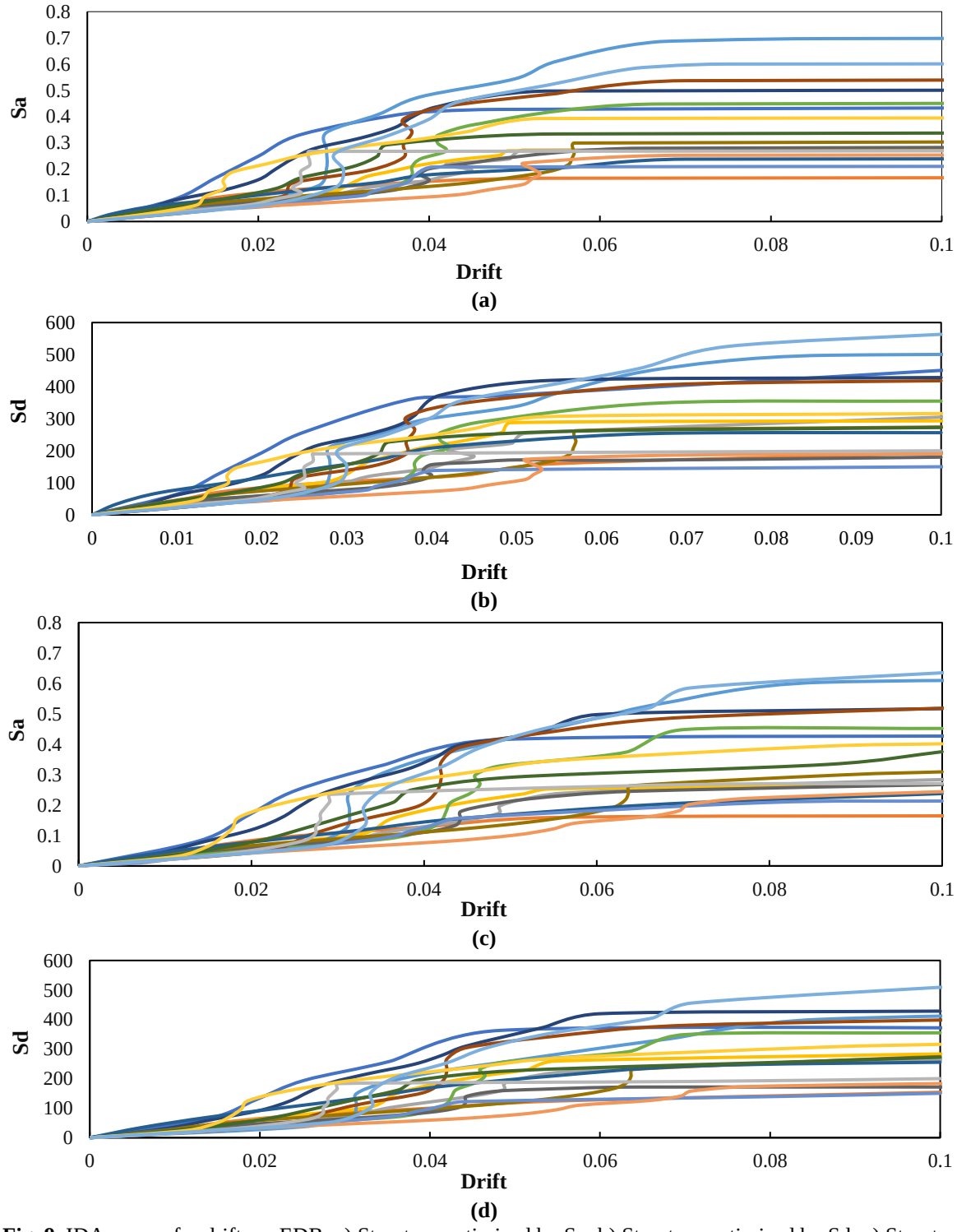

Fig. 9. IDA curves for drifts as EDB: a) Structure optimized by Sa; b) Structure optimized by Sd; c) Structure initialized by Sa; and d) Structures initialized by Sd

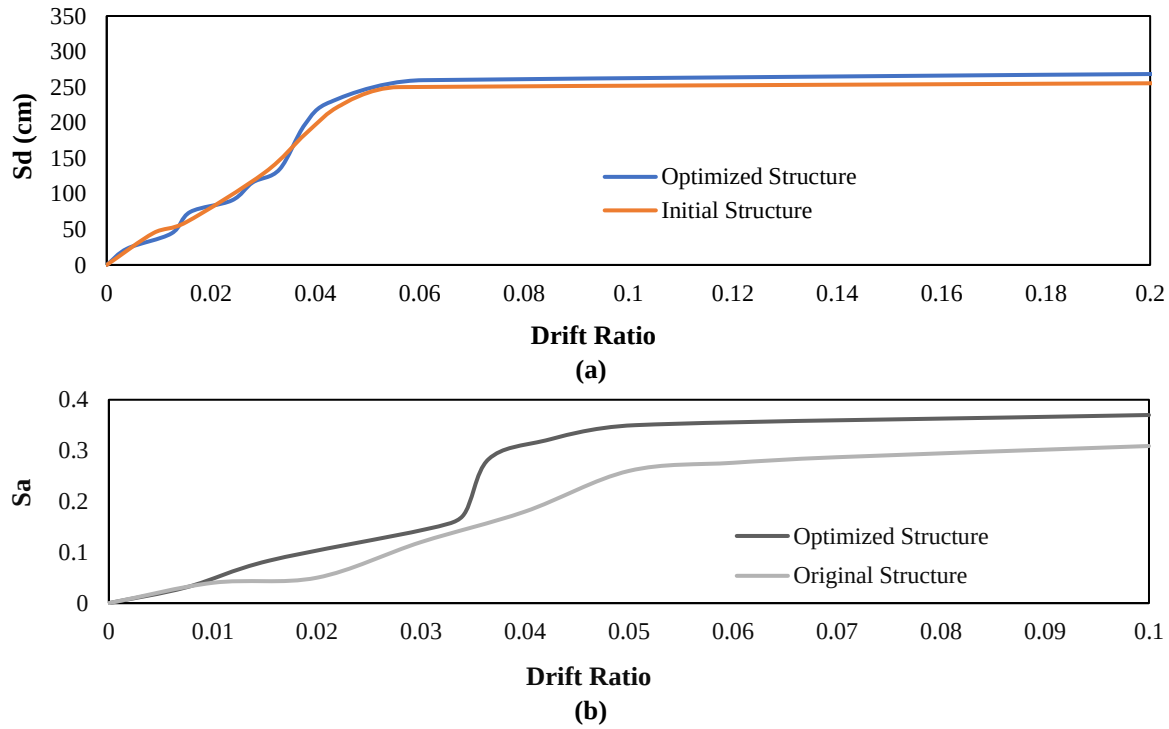

Fig. 10. Median curves derived from IDA analysis for both structures: a) Based on Sd; and b) Based on Sa

An investigation into the variations of IDA curves versus Sa and Sd shows that, in both structural models, the median IDA curve has a softer state versus Sd changes and varies through a significant trend, while the curve shows a hardening state versus Sa changes. Comparison of the curves of both structures also shows that the EDP values of original structure are greater in a given IM, which indicates that the overall performance of optimized outrigger braced structure is better than the conventional structure. Although the ratio of 20% of IDA curve slope to the initial slope is defined as CP performance level according to the FEMA 356, the maximum drift of 0.053 is calculated as CP performance level considering the parameter Sd as IM for both structures. If the parameter Sa is considered IM, the CP performance level is 0.055 for the optimized structure and 0.05 for the original structure. If the end point of elastic range is considered as IO performance level, the drift of IO is 0.0152 with the IM considered in terms of Sd and 0.01 with the IM considered in terms of Sa. For the optimized outrigger braced structure, they are calculated 0.0152 and 0.0154, respectively. Given these two performance levels, Figure 11 shows fragility curves of the structures with Sa and Sd separately considered as IM. According to the figure, the exceedance probability of IO and CP performance levels in the optimized outrigger braced structure is less than that of original structure. An examination of both IMs suggests that if the Sd value is considered as a criterion, the structures have a 10% exceedance probability of IO performance level in near-field earthquakes with an Sd greater than 10 cm; it would equal 100% for the original structure at Sd = 80 cm and for the optimized structure at Sd = 101 cm. In the original structure, the exceedance probability of CP performance level is 10% at Sd = 130 cm and 100% at Sd = 350 cm. In the optimized outrigger braced structure, the exceedance probability of CP performance level is 9% at Sd = 150 cm and 100% at Sd = 400 cm. The results show that the optimization of outrigger bracing placement has a significant effect on the reduction of exceedance probability of IO and CP performance levels in near-field earthquakes. An investigation into fragility curves of the IMs also shows that exceedance probability of CP performance level starts to increase in low Sa values in

both structures; this phenomenon indicates the selection of Sa as IM cannot be a good choice for tall buildings, because the exceedance of CP performance level is probable in very small values of Sa.

4. Evaluation of IDA Curve Considering Plastic Strain Energy as EDP

According to Eq. (1), the input seismic energy applied to the structure is converted into kinetic energy, potential energy and dissipated energy. The potential energy is stored in form of elastic strain energy in the structure (Szyniszewski and Krauthammer, 2012; Moradi and Abdolmohammadi, 2020). The dissipated energy includes the plastic strain energy and the energy dissipated by damping in the structure (Song et al., 2018). If the sum of kinetic, stored and dissipated energies is in balance with the energy input induced by earthquake, the structure remains stable; otherwise the structure is faced with instability. On the other hand, the plastic strain energy causes damage in the structure; the greater the amounts of energy, the more structural members are damaged. Internal energy curves are studied in an earthquake. Figure 12 represents the values of plastic strain energy, elastic strain energy, energy dissipated by damping and kinetic energy in the original and optimized outrigger braced structures in Imperial Valley earthquake at PGA = 1g. The analysis was performed in the range of forced vibration and free vibration was omitted in this study. But since in all records the most drift occurred in the forced vibration range, it makes perfect sense to avoid free vibration. However, the time history curve of plastic strain energy also shows that the curve is horizontal at the end of the analysis, which indicates that the energy lost in the structure was also in the range of forced vibration. Therefore, the hypothesis of not considering free vibration is a correct hypothesis in this research.

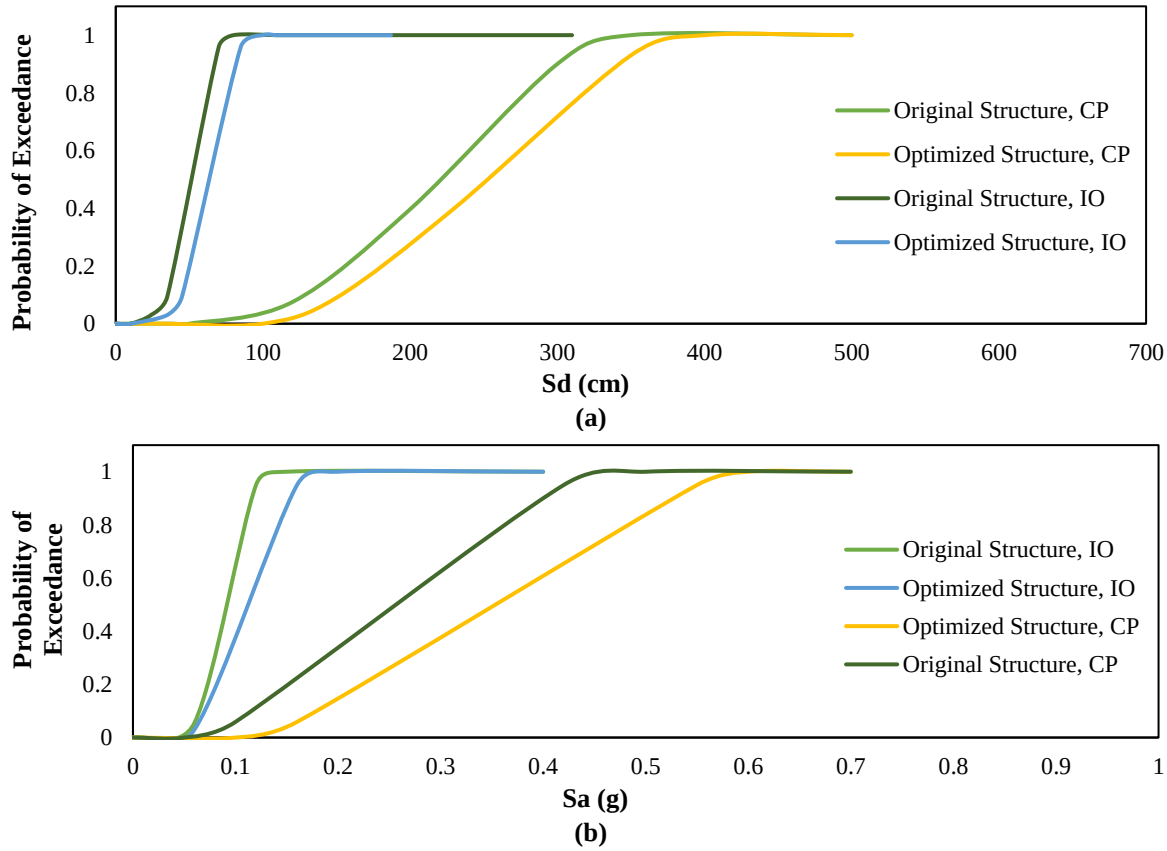

Fig. 11. Fragility curves: a) Considering Sd as IM; and b) Considering Sa as IM

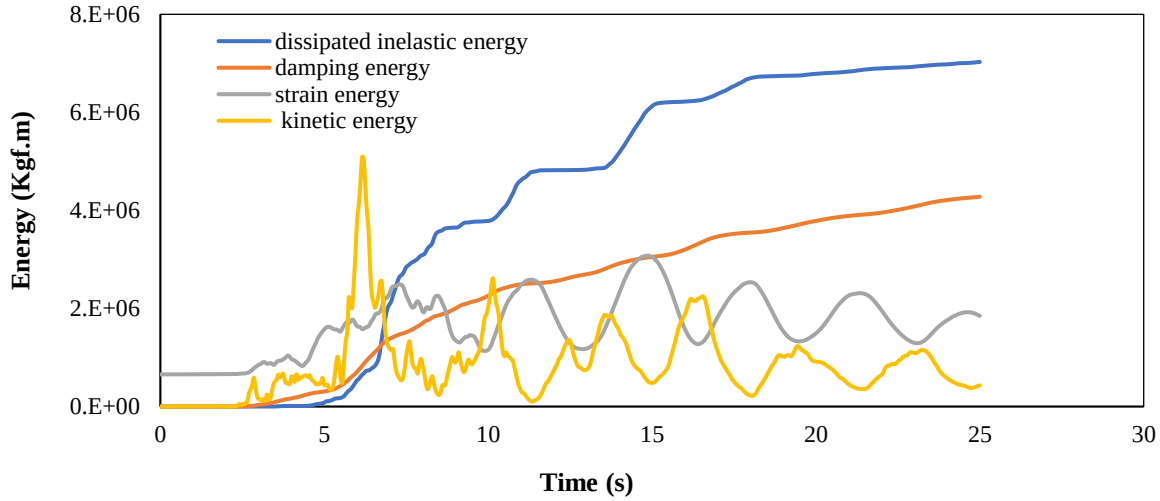
8.E+06
6.E+06
4.E+06
2.E+06
0.E+00
Energy (Kgf.m)
dissipated inelastic energy
damping energy
strain energy
kinetic energy
0
5
10
15
20
25
30
Time (s)

(a)

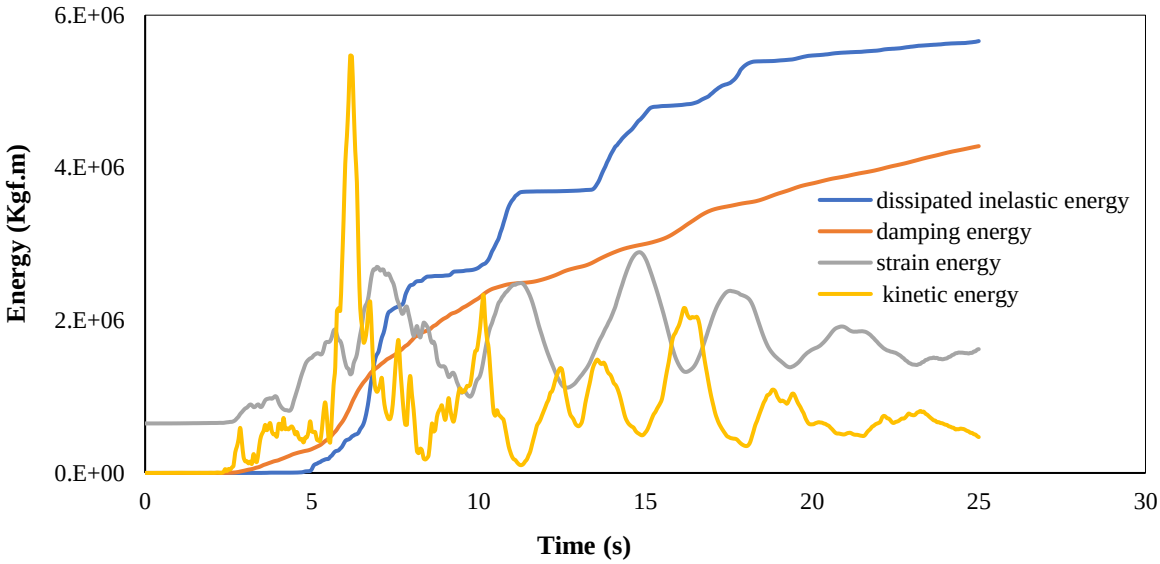
6.E+06
4.E+06
2.E+06
0.E+00
Energy (Kgf.m)
dissipated inelastic energy
damping energy
strain energy
kinetic energy
0
5
10
15
20
25
30
Time (s)

(b)

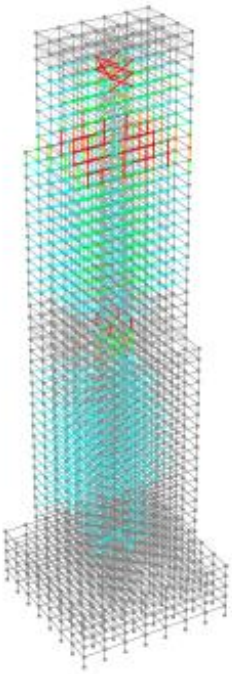

(c)

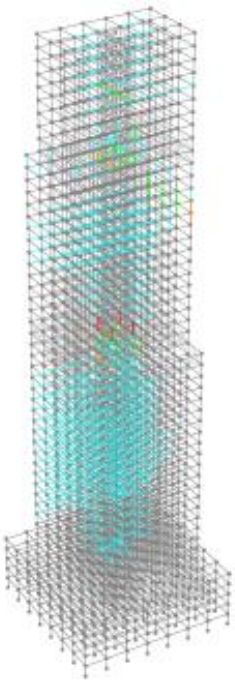

(d)

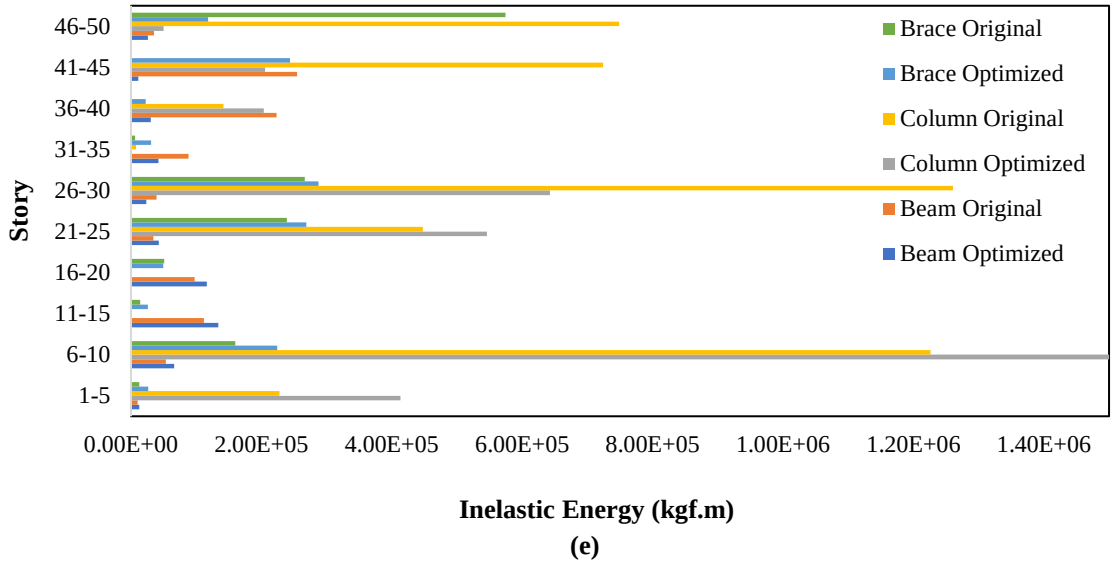

(e)

Fig. 12. a) Energy balance in original structure; b) Energy balance in optimized structure; c) Plastic hinge rotations at LS performance level in original structure; d) Plastic hinge rotations; and e) Distribution of plastic strain energy on floors at LS performance level in optimized structure in Imperial Valley earthquake

The assessment of energy curves in both structures shows that the dissipated energy, the sum of the plastic strain energy and the energy dissipated by damping in the structure has an ascending trend in the energy balance. Elastic strain energy has a limited capacity within the elastic range of structure, partly stored by gravity load of the structure. Hence the elastic strain energy of the structure starts from a non-zero value in the energy balance. An investigation into the energy curves in both structures shows that less energy is dissipated by plastic strain energy in the optimized outrigger braced structure in comparison with the original structure, which indicates that this structure suffers less damage than the original structure. The total strain energy dissipated due to the plastic strain energy is calculated as 5.7e6 kgf.m for the optimized outrigger braced structure and 7e+6 Kgf.m for the original structure. An investigation into the amount of plastic strain energy in the structures shows that the increase of plastic strain energy by 1.3e6 kgf.m causes more elements to enter the LS performance level in the original structure and their periods to exceed the LS performance level. Accordingly, these elements suffer more damage in the original structure in comparison with the optimized outrigger braced structure.

Figure 12e shows the distribution of plastic strain energy for beam, column and bracing elements on different floors. According to the figure, in the original structure, the plastic strain energy of structural elements on most floors is more than that of optimized structure. However, the maximum strain energy occurs in the columns of 6^{th}-10^{th} floors in the optimized structure, which indicates that the structural damage on these floors is more than that for the original structure. But the overall performance of structure in accordance with total plastic strain energy criterion in structures shows that the original structure dissipates more plastic strain energy, resulted in greater structural damage. Two views can be adopted to evaluate the structural performance using plastic strain energy. The first view is to investigate the amount of plastic strain energy on each floor of the structure. The amount can indicate the damage induced to each floor of the structure. The second view is related to the strain energy dissipated in the entire structure, which can also reflect the overall damage to the structure. Therefore, two criteria of EDP and IM can be considered for the strain energy dissipated in each structure. The first criterion is determined

by the energy dissipated on each floor of the structure versus the IM of each floor and the second criterion is determined according to the total energy dissipated in the structure versus the total IM of the structure. The second view can reflect the overall damage to the structure and the exceedance probability of each IM may indicate the collapse probability of the structure. In the following, the strain energy dissipated in the whole structure is considered as EDB and its IDA curves are plotted versus the Sd for both structures (Figure 13).

In Figure 13, an examination of IDA curves shows that the plastic strain energy-Sd curves are composed of three sections. The first section is related to the strain energy of about zero. The plastic strain energy of zero on the IDA curve shows that the structure has elastic behavior at corresponding Sd. In these Sds, the input energy applied to the structure is in the balance with the elastic strain energy, the energy dissipated by damping and the kinetic energy and the elements do not enter the nonlinear range. The IDA curve has an infinite slope in the first section. In the second section of IDA curves, the plastic strain energy occurs in the structure as the Sd increases and the structure enters the plastic range. At this stage, the structure is stable but exposed to damage and the plastic joints emerge in the structure. In this section, the infinite slope of IDA curve decreases gradually. In the third section, the slope of IDA curve moves towards zero. In the third section of this curve, the strain energy increases abruptly and the structure is exposed to instability as the Sd increases. The third section actually represents the plastic strain energy corresponding to the point of structural rupture.

In Figure 14, the median IDA curves are shown versus plastic strain energy in the both structures discussed in this study. According to the figure, the median curves are also composed of three sections, like the main curves. This curve shows that the amount of plastic strain energy for each Sd is greater in the original structure than the optimized outrigger braced structure. If the distance between the second and third sections of median curve is considered as strain energy for the collapse limit, the value can be noticed as a failure criterion in the structure. In fact, the behavior of plastic strain energy versus increasing IM in the structure corresponds to zero in a range, an incremental trend in another range and a sudden increase in the other range; the boundary between the increasing trend and the sudden increase can be considered as a the collapse limit of the structure, which indicates the entire collapse of the structure. In Figure 14, the value is equal to 5.8e7 Kgf.m for both structures. Considering the limit as the collapse limit, the fragility curve can be plotted based on plastic strain energy as EDP.

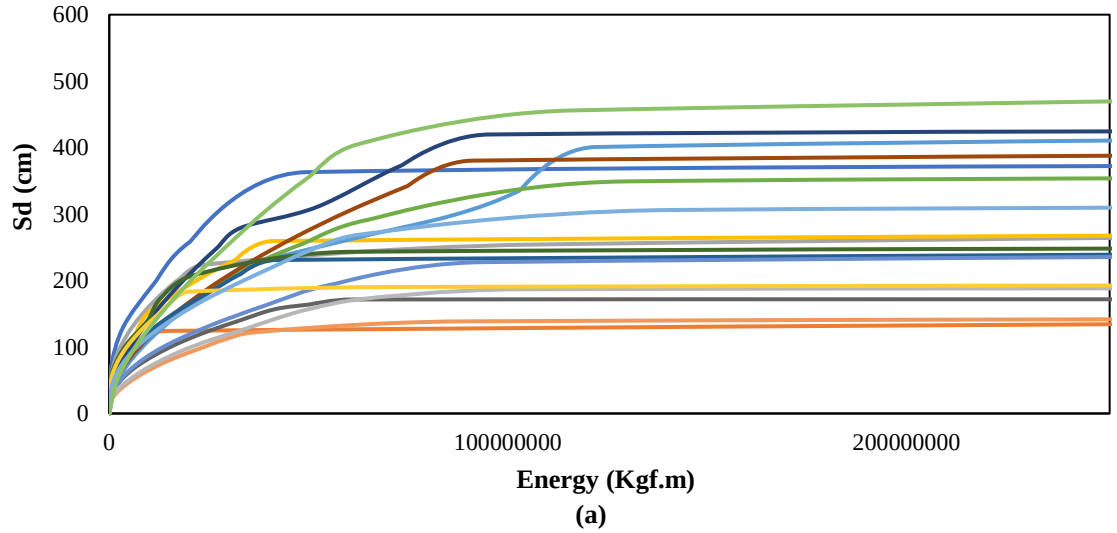

(a)

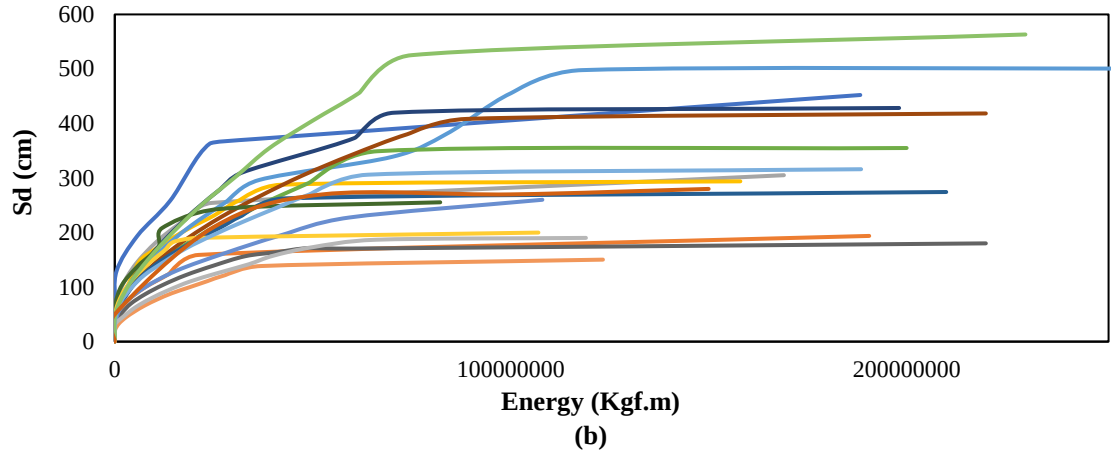

Fig. 13. IDA curve based on plastic strain energy: a) Original structure; b) Optimized structure

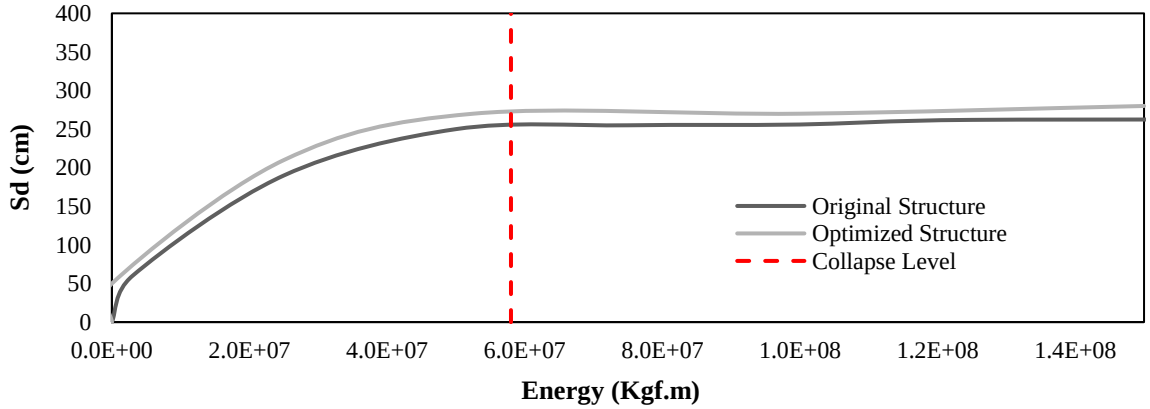

Fig. 14. Median curves derived from IDA curves based on Sd and plastic strain energy

In Figure 15, the fragility curve obtained from the parameter Sd as IM and the plastic strain energy as EDP are derived and presented for both structures discussed in this study. According to the figure, like previous fragility curves, the optimized structure has a lower probability of failure in the same IMs in comparison with the original structure. In the following, the fragility curves of the structures are compared with the drift considered as EDP and the plastic strain energy considered as EDP. According to Figures 11 and 15, the fragility curves with plastic strain energy considered as EDP almost have a good convergence with the fragility curves with drift considered as EDP in the rupture of structure. Therefore, to evaluate the collapse probability in structures, the drift can be substituted by the strain energy criterion as an effective parameter in the assessment of structural damage.

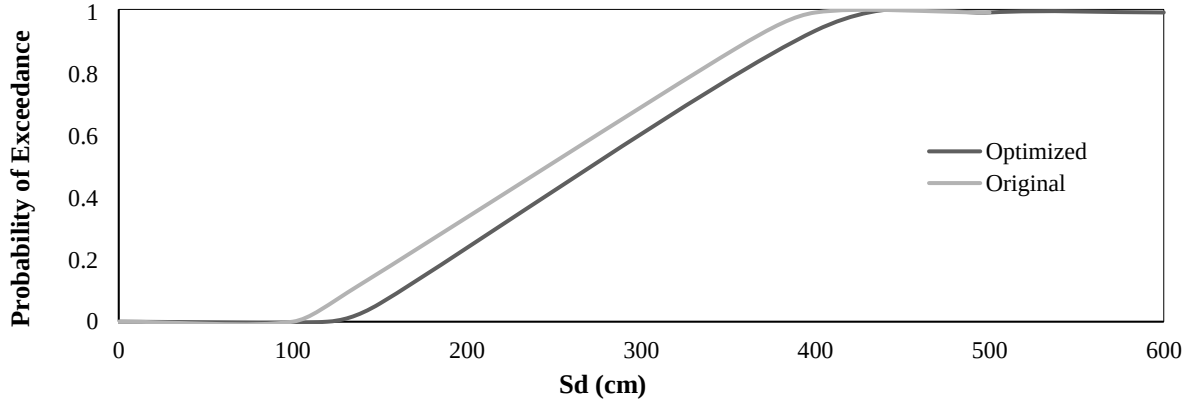

Fig. 15. Fragility curve based on energy and Sd in original and optimized structures

5. Conclusions

Aimed to investigate the effect of optimizing outrigger bracing placement in tall structures, the behavior of this structural system is studied in two structures of 50 floors in this article. In the original model, outrigger braces are placed on the last two and the middle two floors; while in the optimized model, the outrigger braces of the last two floors are transferred to the 42nd and 41st floors after calculations. Many parameters are used to assess the behavior of structures. IDA curves are the most important parameter for evaluating the behavior of structures in this research. Two parameters of maximum story drift and plastic strain energy are considered as EDB and two parameters of Sa and Sd are also considered as IM in fragility curves. The results of analyses are summarized as follows:

- The plastic hinge rotations and maximum story drift show that the optimization of outrigger bracing placement improves the behavior of structure. The process is obvious in the median curves derived from the IDA curves.
- The energy balance shows that the placement of outrigger bracing system is optimized in the structure, the plastic strain energy declines, while the elastic strain energy and the energy dissipated by damping do not change significantly and the kinetic energy may increase. In the optimized structure, the plastic strain energy of most floors is less than that for the original structure.
- The results show that if maximum story drift is selected as EDB and the Sa is considered as IM, the collapse limit in the optimized structure is 5% higher than that of the original structure. However, if the Sd is chosen as IM, the collapse limit is the same in both structures.
- An investigation of fragility curves for both structures shows that the collapse probability of the optimized structure is less than that of the original structure for the same IM. The results of fragility analysis suggest that the collapse probability of 100% is at Sd = 400 cm for the optimized structure and at Sd = 350 cm for the original structure.
- The selection of total plastic strain energy as EDB and its corresponding fragility curves demonstrate that the collapse probability equals 100% at Sd=400 cm in the original structure and at Sd=500 cm in the optimized structure.

6. Acknowledgements

The authors acknowledge the funding support of Babol Noshirvani University of Technology through Grant No. BUT/388011/400.

7. References

ASCE. (2016). *Minimum design loads for buildings and other structures*, American Society of Civil Engineers.

Asgarian, B. and Ordoubadi, B. (2016). "Effects of structural uncertainties on seismic performance of steel moment resisting frames", *Journal of Constructional Steel Research*, 120, 132-142.

Dall'Asta, A., Dabiri, H., Tondi, E. and Morci, M. (2021). "Influence of time-dependent seismic hazard on structural design", *Bulletin of Earthquake Engineering*, 19(6), 2505-2529.

Ding, R., Nie, X., Tao, M.-X. and Fan, J.-S. (2018). "Fishbone-shaped beam–column model for steel outrigger truss-concrete wall composite joints", *Journal of Constructional Steel Research*, 145, 386-396.

FEMA 356, Federal Emergency. (2000). *Prestandard and commentary for the seismic rehabilitation of buildings*, Federal Emergency Management Agency: Washington, DC, USA.

Gorji, M.S. and Cheng, J.R. (2017). "Steel plate shear walls with outriggers, Part I: Plastic analysis and behavior", *Journal of Constructional Steel Research*, 134, 148-159.

Gorji, M.S. and Cheng, J.R. (2017). "Steel plate shear walls with outriggers, Part II: Seismic design and performance", *Journal of Constructional Steel Research*, 137, 311-324.

Jamnani, H.H., Amiri, J.V. and Rajabnejad, H. (2018). "Energy distribution in RC shear wall-frame structures subject to repeated earthquakes", *Soil Dynamics and Earthquake Engineering*, 107, 116-128.

Jiang, H., Li, S. and Zhu, Y. (2017). "Seismic performance of high-rise buildings with energy-

dissipation outriggers", *Journal of Constructional Steel Research*, 134, 80-91.
Lee, S. and Tovar, A. (2014). "Outrigger placement in tall buildings using topology optimization", *Engineering Structures*, 74, 122-129.
Mobinipour, S.A. and Pourzeynali, S. (2020). "Assessment of near-dault ground motion effects on the fragility curves of tall steel moment resisting frames", *Civil Engineering Infrastructures Journal*, 53(1), 71-88.
Mohammadizadeh, M.R. and Jafarzadeh, A. (2021). "Comparison of nonlinear dynamic analysis of time history and endurance time method in tall structures with frame-wall system", *Civil Engineering Infrastructures Journal*, 54(2), 405-421.
Moradi, M. and Abdolmohammadi, M. (2020). "Seismic fragility evaluation of a diagrid structure based on energy method", *Journal of Constructional Steel Research*, 174, 106311.
Nazari, Y.R. and Saatcioglu, M. (2017). "Seismic vulnerability assessment of concrete shear wall buildings through fragility analysis", *Journal of Building Engineering*, 12, 202-209.
Patil, D.M. and Sangle, K.K. (2016). "Seismic behaviour of outrigger braced systems in high rise 2-D steel buildings", In *Structures*, Elsevier, 8, 1-16.
Shin, D.-H. and Kim, H.-J. (2016). "Influential properties of hysteretic energy dissipating devices on collapse capacities of frames", *Journal of Constructional Steel Research*, 123, 93-105.
Song, Z., Frühwirt, T. and Konietzky, H. (2018). "Characteristics of dissipated energy of concrete subjected to cyclic loading", *Construction and Building Materials*, 168, 47-60.
Stafford Smith, B. and Coull, A. (1991). *Tall building structures: Analysis and design*, Wiley-Interscience.
Szyniszewski, S. and Krauthammer, T. (2012). "Energy flow in progressive collapse of steel framed buildings", *Engineering Structures*, 42, 142-153.
Tajammolian, H., Khoshnoudian, F., Rad, A.R. and Loghman, V. (2018). "Seismic fragility assessment of asymmetric structures supported on TCFP bearings subjected to near-field earthquakes", In *Structures*, Elsevier, 13, 66-78.
Tan, P., Fang, C., Chang, C. Spencer, B. and Zhou, F. (2015). "Dynamic characteristics of novel energy dissipation systems with damped outriggers", *Engineering Structures*, 98, 128-140.
Tavakoli, H. and Afrapoli, M.M. (2018). "Robustness analysis of steel structures with various lateral load resisting systems under the seismic progressive collapse", *Engineering Failure Analysis*, 83, 88-101.
Zhao, E., Cheng, K., Sun, W., Zhou, Z. and Zhao, J. (2017). "Buckling failure analysis of truck mounted concrete pump's retractable outrigger", *Engineering Failure Analysis*, 79, 361-370.